SENSITIVITY OF REGIONAL CLIMATE MODELLING OVER RAGGED TERRAIN OF ETHIOPIA TO BOUNDARY FORCING

By

GIRMA MOLORO

SUBMITTED IN PARTIAL FULFILLMENT OF THE
REQUIREMENTS FOR THE DEGREE OF
MASTER OF SCIENCE IN PHYSICS
AT
ADDIS ABABA UNIVERSITY
ADDIS ABABA, ETHIOPIA
JULY 06 2010

ADDIS ABABA UNIVERSITY
DEPARTMENT OF
PHYSICS

Supervisor: _____
Dr. Gizaw Mengistu

Examiners: _____
Prof. A.V. Gholap

_____
Dr. Lemi Demeyu

ADDIS ABABA UNIVERSITY

Date: **JULY 06 2010**

Author: **GIRMA MOLORO**

Title: **SENSITIVITY OF REGIONAL CLIMATE MODELLING OVER RAGGED TERRAIN OF ETHIOPIA TO BOUNDARY FORCING**

Department: **Physics**

Degree: **M.Sc.** Convocation: **JULY** Year: **2010**

Permission is herewith granted to Addis Ababa University to circulate and to have copied for non-commercial purposes, at its discretion, the above title upon the request of individuals or institutions.

Signature of Author

Dedicated to my lovely wife W/ro Yitaktu Hando and our child Mieraf Girma. My dear wife devote her life to support me to accomplish this Master of degree successfully. I wish long live and success throughout her life to Nunuye.

Table of Contents

List of Figures

Acknowledgements

Above all, I would like to thank the almighty; God, for letting me accomplish this stage and for giving a good family, especially Ato Hando Deffo and W/ro Zenebech Manulo. They carry out all my duties during my stay in the university. So, they are independent persons for me and for Mieraf Girma (Nunu).

I would like to thank my advisor Dr. Gizaw Mengistu for his timeless help through out the year. With out his effort the thesis should not have been completed. Dr. Gizaw was always there to listen and to give advice. He showed me different ways to approach a research problem and the need to be persistent to accomplish any goal.

I sincerely appreciate Dr. Gulilat Tefera Diro for his support in suggesting solution during RegCM3 test runs. I would also like to acknowledge him for suggesting to work in this direction.

I thank my brother Ato Solomon Moloro. He has done all what he can for my education more than any best brother has done for his brother to fulfill my interest starting from the elementary education to this level. I am also highly indebted to my father Ato Moloro Abega, my mother W/ro Checho Ejo, and my sister Aregash Moloro. They lead me in a good way. I also appreciate Ato Taddese Wake and his wife Aster Hando for their regular encouragement during my stay in the university.

I deeply thanks my lovely wife W/ro Yitaktu Hando (Tatye). She is the hero of my success.

GOD IS GOOD ALL THE TIME!!!

Abstract

The RegCM3 rainfall simulations based on the three boundary forcing fields ERA40, ERAIN and NNRP1 have been compared with observational rainfall over Ethiopia for the period from 1989−1999. The RegCM3 simulations are carried out for all three boundary fields with the same horizontal resolution (60 km), domain size and model physics. The performance of RegCM3 in capturing major large scale features, interannual, interseasonal and intraseasonal variability over the simulation period is found to be good. However, the RegCM3 simulation based on ERA−INTERIM has captured the features better than the other two throughout the simulation period. The precipitation from RegCM3 agree well with the observed precipitation in general. Comparison of the simulations carried out using the three forcing fields reveals that simulation of rainfall based on ERA−INTERIM boundary forcing reproduces observed precipitation from CRU dataset better than the other two simulations. ERA40 and NNRP1 simulation have shown a negative rainfall bias compared to the CRU rainfall for some homogeneous regions of Ethiopia.

Chapter 1

Introduction

The International Center for Theoretical Physics (ICTP) Regional Climate Model, RegCM3 performs adequately in simulating the mean and interannual variability of the climate and investigate the impact of land cover changes (desertification and deforestation) on the West African monsoon and rainfall patterns over the region by ([1], and references therein). Regional climate models (RegCM3) have become increasingly important tools in the study of regional climate patterns and processes and for downscaling global climate information for regional applications. RegCM3 are used to study regional climate variability at different timescales and to increase our understanding of the roles that mesoscale and regional−scale climate processes play in shaping the atmospheric response to surface and lateral boundary forcing.

Regional Climate Model (RegCM3) has been utilized extensively for mid−latitude regions in wide ranging surface climate and hydrologic process investigations, sensitivity studies, and simulations of past, present, and future climates on the mesoscale and regional scale. An improved and enhanced version of RegCM3 now is run at the Abdus Salam International Center for Theoretical Physics (ICTP), with particular focus on regional climate variability in developing nations. Although the NCAR RegCM2/ICTP RegCM3

has been applied to regional climates in near−equatorial East Africa ([2], and reference therein).

Simmons et al. (2004) ([2], and references therein) compared global surface air temperature anomalies from CRUTEM2v (Climatic Research Unit Temperature version 2 variance corrected) with ERA-40 and NNRP-1. They found that ERA-40 showed better agreement with CRUTEM2v than NNRP-1 over the time periods 1958−2001 and 1979−2001. In addition, they reported closer agreement between ERA-40 and CRUTEM2v over the period 1979−2001 compared with the period 1958−1979. This was attributed to the greater observational coverage after 1979 which is linked to the inclusion of satellite data

.

The general objective of this study is to assess the influence of forcing fields from different dataset on the performance of regional climate modeling (RegCM3).

The specific objectives of the study are

- to use ERA40, ERA−INTERIM and NNRP1 dataset as initial and boundary values of RegCM3 simulation over Ethiopia;
- to assess the influence of the dataset on the simulation results, in particular their role on improving the accuracy of the simulated precipitation field.
- to determine the best dataset for boundary forcing over ragged terrain of Ethiopia for future climate research.

In view of the above stated objectives, this study discuss comparison of the RegCM3 precipitation disturibution based on the boundary forcing field from ERA40, ERA−INTERIM

and NNRP−1 dataset with observational data (CRU) over Ethiopia for the period 1989−1999. The period 1989−1999 was chosen because all four dataset have data during this period.

The outline of the thesis is as follows. Chapter 2 covers atmospheric dynamics and its implimentation in RegCM3. Chapter 3 discusses the RegCM3 and experimental design of this thesis while chapter 4 gives overview of dataset used for boundary forcing and data analysis tools. Chapter 5 discusses the results of our simulation and finally conclusion is given in chapter 6.

Chapter 2

Dynamics of the atmosphere

This section presents the basic model equations, conservation laws of atmospheric dynamics and the vertical and horizontal coordinate system.

2.1 Basic conservation laws of atmospheric motion

Atmospheric motions are governed by three fundamental conservation principles. These are conservation of mass, conservation of momentum and conservation of energy. The mathematical relationship between these laws can be derived by considering the amount of mass content, momentum content and energy content for an infinitesimal control volume. Two types of control volume are commonly used in atmospheric dynamics; Eulerian and Lagrangian frame of reference. Eulerian frame of reference consists of a parallelepiped of sides δx, δy, δz whose positions are fixed relative to the coordinate axes. The amount

of mass, momentum and energy contents will depend on fluxes caused by the flow of atmospheric parcel through the boundaries of the volume. But, in the case of Lagrangian frame the control volume of the atmosphere moves following the motion of the fluid, always containing the same particles [3].

The conservation laws of atmosphere to be derived contain expression for the rate of change of density, momentum and thermodynamic energy following the motion of particular fluid parcel. In order to use Eulerian frame, it is necessary to derive a relationship between the rate of change of a fixed variable following the motion and its rate of change at a fixed position. That means, the Eulerian is the time derivative at a fixed location. The position of an air parcel is given by (x,y,z) and is a function of time so, x=x(t), y=y(t), and z=z(t). We can relate the total change in the field variable temperature (δT) as a function of time[i.e T(x,y,z,t)] to changes at a fixed location [4]. If the air parcel moves its position becomes $x_o \to x_o + \delta$x, $y_o \to y_o + \delta$y, $z_o \to z_o + \delta$z and t $\to \delta$t. Then the temperature change of the parcel can be expressed in Taylor series as

$$\delta T = (\frac{\partial T}{\partial t})\delta t + (\frac{\partial T}{\partial x})\delta x + (\frac{\partial T}{\partial y})\delta y + (\frac{\partial T}{\partial z})\delta z + higherorderterm \tag{2.1.1}$$

Dividing both side by δt and taking the limit δt goes to zero gives

$$\frac{DT}{Dt} = \frac{\partial T}{\partial t} + (\frac{\partial T}{\partial x})\frac{Dx}{Dt} + (\frac{\partial T}{\partial y})\frac{Dy}{Dt} + (\frac{\partial T}{\partial z})\frac{Dz}{Dt} \tag{2.1.2}$$

where $\frac{DT}{Dt}$=$\lim_{\delta t \to 0}$ $\frac{\delta T}{\delta t}$, $\frac{Dx}{Dt}$ =u, $\frac{Dy}{Dt}$=v, $\frac{Dz}{Dt}$=w that

$$\frac{DT}{Dt} = \frac{\partial T}{\partial t} + u(\frac{\partial T}{\partial x}) + v(\frac{\partial T}{\partial y}) + w(\frac{\partial T}{\partial z}) \tag{2.1.3}$$

Using vector notation this expression can be written as

$$\frac{DT}{Dt} = \frac{\partial T}{\partial t} + \vec{U} \cdot \nabla T \tag{2.1.4}$$

where $\vec{U}$= u$\hat{i}$ + v$\hat{j}$ + w$\hat{k}$ and $\nabla T = \frac{\partial T}{\partial x}\ \hat{i} + \frac{\partial T}{\partial y}\hat{j} + \frac{\partial T}{\partial z}\hat{k}$

Only u, v and w are velocity components in x, y, z directions, respectively. So, the local rate of change of temperature equals to the rate of change of temperature following the motion (i.e; heating or cooling of individual air parcel) plus the advective rate of change of temperature i.e.

$$\frac{\partial T}{\partial t} = \frac{DT}{Dt} - \vec{U} \cdot \nabla T \tag{2.1.5}$$

where $\vec{U} \cdot \nabla T$ is temperature advection. It gives the contribution to the local temperature due to air motion. Contribution of advective temperature can be positive or negative. Warm air advection− warmer air is replacing cooler air at a given location and Cold air advection− cooler air is replacing warmer air at a given location it has a negative contribution. The relationship between the total derivative and local derivative given for temperature holds for any of the field variables.

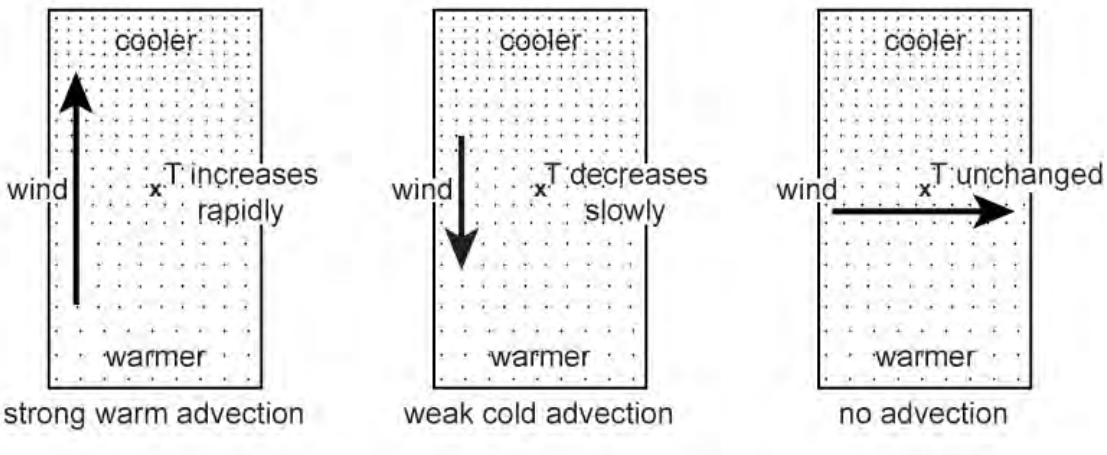

Figure 2.1: Shows temperature advection and its dependence on wind field.

2.1.1 Conservation of mass

One of the fundamental principal governing atmospheric motion is conservation of mass. The equation expressed based on the continuity equation. The continuity equation can be expressed in two ways: Eulerian and Lagrangian. We will consider the Eulerian derivation. Let's consider a volume $\delta x\ \delta y\ \delta z$ that is fixed in space.

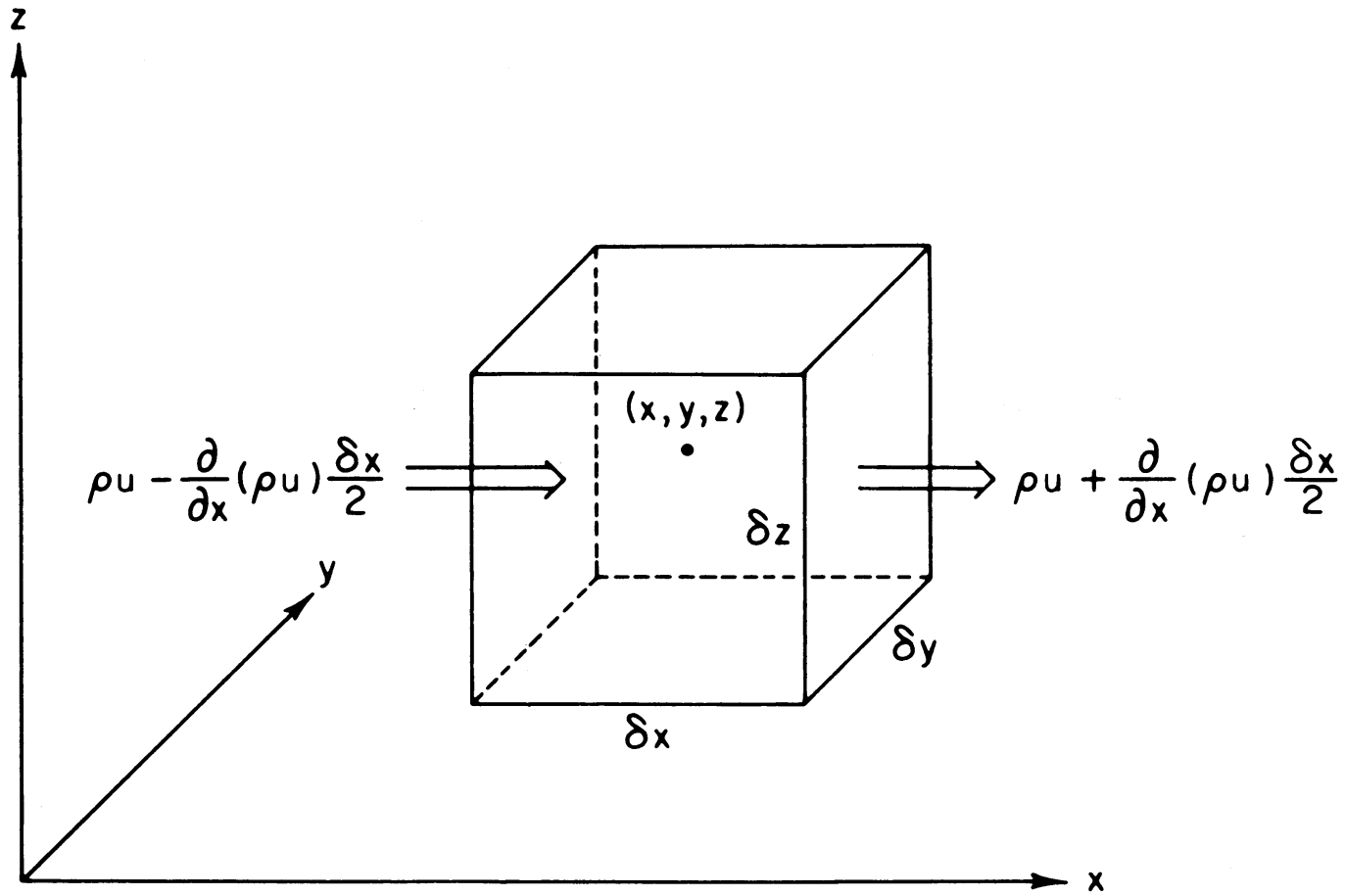

Figure 2.2: Mass inflow into a fixed control volume and mass outflow from a fixed control volume due to motion parallel to the x axis.

Atmospheric mass can flow into and out of this volume due to the wind. We want to know how much mass is coming into the volume and how much is leaving. The amount of mass entering the volume in the left side over time is

$[\rho \text{u} - \frac{\partial(\rho u)}{\partial x} \frac{\delta x}{2}] \delta y \ \delta z$

where u is wind velocity in the x-direction (eastward), ρ is density of air mass, δt is amount of time elapsed. The mass flux out of the right face is given by

$[\rho \text{u} + \frac{\partial(\rho u)}{\partial x} \frac{\delta x}{2}] \delta y \ \delta z$

The first term (ρu) is just the amount that came in from left side of volume and the second term($\frac{\partial(\rho u)}{\partial x} \frac{\delta x}{2}$) is how much mass flow has changed in the x-direction over a distance δx.

The rate of mass change in the volume due to these fluxes is

$\frac{\partial M}{\partial t}$=$\{ [\rho \text{u} - \frac{\partial(\rho u)}{\partial x} \frac{\delta x}{2}] - [\rho \text{u} + \frac{\partial(\rho u)}{\partial x} \frac{\delta x}{2}] \} \delta y \ \delta z$

$\frac{\partial M}{\partial t}$= -$\frac{\partial(\rho u)}{\partial x} \delta x \ \delta y \ \delta z$ this for a single face.

Considering all three faces of this volume gives

$\frac{\partial M}{\partial t}$ = -$[\frac{\partial(\rho u)}{\partial x} + \frac{\partial(\rho v)}{\partial y} + \frac{\partial(\rho w)}{\partial z}] \delta x \delta y \delta z$

Dividing by the volume $[\delta x \delta y \delta z]$ gives the rate of change of density:

$\frac{\partial \rho}{\partial t}$ = -$[\frac{\partial(\rho u)}{\partial x} + \frac{\partial(\rho v)}{\partial y} + \frac{\partial(\rho w)}{\partial z}]$ Therefore

$$\frac{\partial \rho}{\partial t} = -\nabla \cdot (\rho \vec{U}) \tag{2.1.6}$$

This equation is the mass derivative form of the continuity equation, and states that the local rate of change of density is equal to minus the mass divergence. Eq.(2.1.6) can also be expressed by using the following identity property:

$\nabla \cdot (\rho \vec{U}) = \rho \nabla \cdot \vec{U} + \vec{U} \cdot \nabla \rho$

and relationship given in Eq.(2.1.4) as

$$\frac{1}{\rho}\frac{D\rho}{\partial t} + \nabla \cdot \vec{U} = 0 \tag{2.1.7}$$

Eq.(2.1.7) refers to the velocity divergence form of the continuity equation, and states that the fractional rate of density change following the motion is equal to minus the velocity divergence.

2.1.2 Conservation of momentum

Atmospheric motion are also governed by Newton's 2^{nd} law of motion which is stated as "the rate of change of momentum of an object equals to the sum of all forces acting on it". i.e.

$$\frac{D\vec{U}}{Dt} = \sum \vec{F} \tag{2.1.8}$$

This equation is the Newton's 2^{nd} law for air parcel per unit mass in non-inertial earth's reference frame. The right hand side of Eq.(2.1.8) is the sum of all forces acting on the air parcel. While, the left hand side of the equation is the rate of change of absolute velocity following the motion [3].

These forces can be classified as body forces and surface forces. Body forces acts on the center of mass of air parcel and their magnitudes are proportional to the mass of the parcel, like gravity. Surface force act across the boundary surface surrounding a fluid parcel from its surrounding and their magnitudes are independent of the mass of the parcel, like pressure force .

For large scale atmospheric motion pressure gradient force, gravitational force, Coriolis force and frictional forces are dominant forces. So, we can rewrite Newton's 2^{nd} law for

the air parcel in motion as

$$\frac{D\vec{U}}{Dt} = -2\Omega X\vec{U} - \frac{1}{\rho}\nabla P + \vec{g} + \vec{F_r} \tag{2.1.9}$$

The term ($-2\Omega X\vec{U}$) is the deflecting Coriolis force due to the rotation of the earth that the atmosphere experiences. The second term ($\frac{1}{\rho}\nabla P$) is the pressure gradient force acting on the surface which arises as a result of pressure difference. The third term ($\vec{g}$) is the centrifugal force which arises due to the spherical shape of the earth and acts out ward from the axis. The last term ($\vec{F_r}$) is the frictional force because of the normal and tangential stress on the surface. The pressure gradient and frictional forces are surface forces and the rest are body forces. Finally the term from the left hand side ($\frac{D\vec{U}}{Dt}$) is the sum of the local rate of change of velocity and the advection term.

2.1.3 Conservation of energy

The third fundamental principle of atmospheric dynamics is the conservation of energy which described interns of first law of thermodynamics. Thus, the first law of thermodynamic state that "the change in internal energy of the system is equal to the difference between the heat added to the system and the work done by the system".i.e.

$$dU = dQ - dW \tag{2.1.10}$$

When heat is added to the system some of it is used to change the internal energy (and temperature) and the rest is used by the parcel of air to do work. Energy exchange (or transformation) can occurr upon the change of state of substance. So, energy is released to the system (air parcel) during condensation of water vapor, freezing of liquid water,

exothermic chemical reaction and radiative decay. Energy is also removed from the system upon melting of ice, sublimation of ice, and evaporation of liquid water [4, 5].

The energy exchange equations in the atmosphere can be derived by combining the first law of thermodynamics with continuity equation for an air parcel. The first law of thermodynamics Eq.(2.1.13) can be rewritten as

$dQ = C_v\mathrm{dT} + \mathrm{Pd}\alpha$

Since $\mathrm{d(P}\alpha) = \mathrm{Pd}\alpha + \alpha\mathrm{dP}$, we can rewrite the above equation as

$dQ = C_v\mathrm{dT} + \mathrm{d(P}\alpha)$ - $\alpha\mathrm{dP}$,

$dQ = (C_v + R)dT + \alpha dP.$

Using equation of state $P\alpha = RT$, we obtain

$dQ = C_p dT - \alpha dP$

By substituting $\alpha = \frac{1}{\rho}$, and rearranging this gives the thermodynamic energy equation:

$$dT = \frac{1}{C_p}dQ + \frac{1}{\rho C_p}dP \tag{2.1.11}$$

2.2 Conservation laws as implemented in regional climate model (RegCM3)

2.2.1 Sigma coordinate

The sigma coordinate system defines the base at the model's ground level, and the surfaces of the coordinate variable do not intersect ground topography. The surface in the

sigma coordinate system follow the model terrain and are steeply sloped in the regions when terrain itself is steeply sloped. It describes the vertical position of a point in the atmosphere as a rate of the pressure difference between that point and the top of the domain to that of the pressure difference between a fundamental base below the point and the top of the domain [6]. The sigma coordinate is defined as

$$\sigma = \frac{P - P_{top}}{P_{surface} - P_{top}} = \frac{P - P_{top}}{P^*} \tag{2.2.1}$$

It can be seen from Eq.(2.2.9) and Fig. 2.3 that σ is zero at the top and one at the

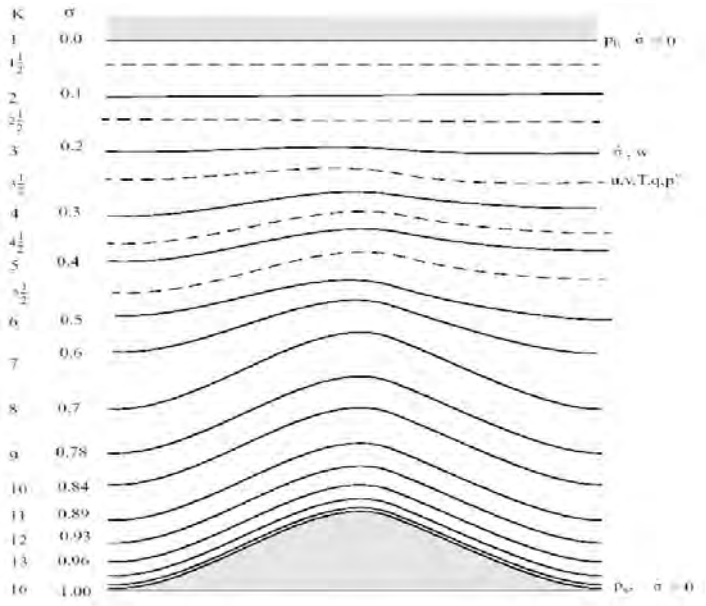

Figure 2.3: Schematic representation of the vertical structure of the model. This example is for 16 vertical layers. Dashed lines denote half-sigma levels, solid lines denote full-sigma levels .

surface. The model vertical resolution is defined by a list of values between zero and one that do not necessarily have to be evenly spaced. Surface pressure varies over the surface of the earth with the height above sea level, and it also varies due to weather. The surface pressure is approximately 1013 hPa at sea level but is significantly lower in a high region.

2.2.2 Horizontal coordinate

The horizontal grid has an Arakawa-Lamb B-staggering of the velocity variables with respect to the scalar variables. This is shown in Fig. 2.4 where it can be seen that the scalars (T, q, p, etc) are defined at the center of the grid box, while the eastward (u) and northward (v) velocity components are collocated at the corners. The center points of grid squares will be referred to as cross points, and the corner points are dot points. Hence horizontal velocity is defined at dot points. Data is input to the model; the preprocessors do the necessary interpolation to assure consistency with the grid [6].

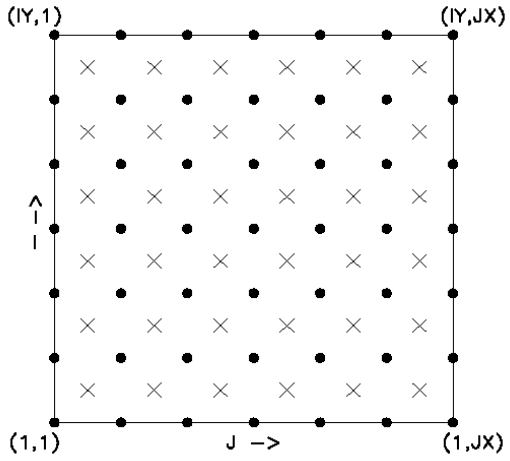

Figure 2.4: Schematic representation showing the horizontal Arakawa B-grid staggering of the dot and cross grid points .

2.2.3 Momentum equations

The vertical coordinate of the RegCM3 model is the terrain-following σ coordinate shown in Fig. 2.3. The equations of motion for this system are:

$$\frac{\partial p^* u}{\partial t} = -m^2(\frac{\partial p^* uu/m}{\partial x}+\frac{\partial p^* vu/m}{\partial y})-\frac{\partial p^* u\dot{\sigma}}{\partial \sigma}-mp^*[\frac{RT_v}{(p^*+p_t/\sigma)}\frac{\partial p^*}{\partial x}+\frac{\partial \phi}{\partial x}]+fp^* v+F_H u+F_V u \tag{2.2.2}$$

$$\frac{\partial p^* v}{\partial t} = -m^2(\frac{\partial p^* uv/m}{\partial x}+\frac{\partial p^* vv/m}{\partial y})-\frac{\partial p^* v\dot{\sigma}}{\partial \sigma}-mp^*[\frac{RT_v}{(p^*+p_t/\sigma)}\frac{\partial p^*}{\partial y}+\frac{\partial \phi}{\partial y}]+fp^* u+F_H v+F_V v \tag{2.2.3}$$

where u and v are the eastward and northward components of velocity, T_v is virtual temperature, ϕ is geopotential height, f is the Coriolis parameter, R is the gas constant for dry air, m is the map scale factor for either the polar stereographic, Lambert conformal, or Mercator map projection, $\dot{\sigma} = \frac{d\sigma}{dt}$, F_H and F_V represent the effect of horizontal and vertical diffusion and $p^* = p_{surface} - p_{top}$. The map scale factor m is given by

$$\text{m} = \frac{distanceongrid}{actualdistanceonEarth}$$

2.2.4 Thermodynamic and omega (ω) equations

The thermodynamic equation can be described by differentiating Eq.(2.1.11) with respect to time:

$$\frac{dT}{dt} = \frac{1}{C_p}\frac{dQ}{dt} + \frac{1}{\rho C_p}\frac{dP}{dt} \tag{2.2.4}$$

or

$$\frac{\partial T}{\partial t} = -u\frac{\partial T}{\partial x} - v\frac{\partial T}{\partial y} - w\frac{\partial T}{\partial z} + \frac{1}{C_p}\frac{dQ}{dt} + \frac{1}{\rho C_p}\frac{dP}{dt} \tag{2.2.5}$$

The heating rate ($\frac{dQ}{dt}$) computed from the heating rate due to condensation/evaporation, melting/freezing, sublimation/deposition, and short/long wave radiation is given by

$$\frac{dQ}{dt} = \sum \frac{dQ}{dt} = \frac{dQ_{c/e}}{dt} + \frac{dQ_{m/f}}{dt} + \frac{dQ_{s/d}}{dt} + \frac{dQ_{sw}}{dt} + \frac{dQ_{lw}}{dt} \tag{2.2.6}$$

The resulting thermodynamic equation is

$$\frac{\partial p^* T}{\partial t} = -m^2(\frac{\partial p^* uT/m}{\partial x} + \frac{\partial p^* vT/m}{\partial y}) - \frac{\partial p^* T\dot{\sigma}}{\partial \sigma} + \frac{RT_v\omega}{C_{pm}(\sigma + p_t/p^*)} + \frac{p^* Q}{C_{pm}} + F_H T + F_V T \tag{2.2.7}$$

where C_{pm} is the specific heat for moist air at constant pressure, Q is the diabetic heating, $F_H T$ represents the effect of horizontal diffusion, $F_V T$ represents the effect of vertical mixing and dry convective adjustment, and ω is given by $\omega = p^*\dot{\sigma} + \sigma\frac{dp^*}{dt}$

where

$$\frac{dp^*}{dt} = \frac{\partial p^*}{\partial t} + m(u\frac{\partial p^*}{\partial x} + v\frac{\partial p^*}{\partial y}) \tag{2.2.8}$$

The expression for C_{pm} is

$$C_{pm} = C_p(1 + 0.8q_v) \tag{2.2.9}$$

where C_p is the specific heat at constant pressure for dry air and q_v, is the mixing ratio of water vapor.

2.2.5 Continuity and sigmadot($\dot{\sigma}$) equation

The continuity equation for the model can be written as

$$\frac{\partial P^*}{\partial t} = -m^2[\frac{\partial P^* u/m}{\partial x} + \frac{\partial P^* v/m}{\partial y}] - \frac{\partial P^*\dot{\sigma}}{\partial \sigma} \tag{2.2.10}$$

To compute the temporal variation of the surface pressure in the model, take the vertical integral of Eq.(2.2.10) with respect to dσ:

$$\frac{\partial P^*}{\partial t} = -m^2 \int_0^1 [\frac{\partial P^* u/m}{\partial x} + \frac{\partial P^* v/m}{\partial y}]d\sigma \tag{2.2.11}$$

After calculation of the surface-pressure tendency $\frac{\partial P^*}{\partial t}$, the vertical velocity in sigma coordinates σ is computed at each level in the model from the vertical integral of Eq.(2.2.10).

$$\dot{\sigma} = -\frac{1}{p^*}\int_0^{\sigma}[\frac{\partial P^*}{\partial t} + m^2(\frac{\partial P^* u/m}{\partial x} + \frac{\partial P^* v/m}{\partial y})]d\sigma^{'} \tag{2.2.12}$$

where $\sigma^{'}$ is a dummy variable of integration and $\dot{\sigma}(\sigma = 0) = 0$.

Chapter 3

Regional climate modeling

Climate varies across a wide range of temporal and spatial scales. Yet, climate modeling has long been approached using global models that can model only the broad scales of atmospheric circulations and their interaction with convective cells, land, ocean circulation, and other environmental variables. An alternative to global modeling is regional climate modeling. As the name implies, a regional climate model (RegCM) does not attempt to simulate the entire globe but only a small portion.

3.1 RegCM3

The first generation NCAR RegCM (Regional Climate Model) was built upon the NCAR-Pennsylvania State University (PSU) Mesoscale Model version 4 (MM4) in the late 1980s ([6] and reference therein). The dynamical component of the model originated from the MM4, which is a compressible, finite difference model with hydrostatic balance and vertical σ-coordinates. Later, the use of a split-explicit time integration scheme was added along with an algorithm for reducing horizontal diffusion in the presence of steep topographical gradients. As a result, the dynamical core of the RegCM is similar to that

of the hydrostatic version of Mesoscale Model version 5 (MM5) ([6] and reference therein). For application of the MM4 to climate studies, a number of physics parameterizations were replaced, mostly in the areas of radiative transfer and land surface physics, which led to the first generation RegCM. The first generation RegCM included the Biosphere-Atmosphere Transfer Scheme, BATS, for surface process representation, the radiative transfer scheme of the Community Climate Model version 1 (CCM1), a medium resolution local planetary boundary layer (PBL) scheme, the Kuo-type cumulus convection scheme of Anthes, 1977 [6] and the explicit moisture scheme of Hsie et al. 1984 [6].

A first major upgrade of the model physics and numerical schemes was documented by ([6] and reference therein), and resulted in a second generation RegCM, hereafter referred to as Regional Climate Model version 2 (RegCM2). The physics of RegCM2 was based on that of the NCAR Community Climate Model version 2 (CCM2), and the mesoscale model MM5. In particular, the CCM2 radiative transfer package was used for radiation calculations, the non local boundary layer scheme of Holtslag et al., (1990) [6] replaced the older local scheme, the mass flux cumulus cloud scheme of Grell, (1993) [6] was added as an option, and the latest version of BATS1E was included in the model. In the last few years, some new physics schemes have become available for use in the RegCM, mostly based on physics schemes of the latest version of the Community Climate Model version 3 (CCM3). The CCM3 scheme retains the same structure as that of the CCM2, but it includes new features such as the effect of additional greenhouse gases (NO_2, CH_4, CFCs), atmospheric aerosols, and cloud ice. The other primary changes are in the areas of cloud and precipitation processes. The original explicit moisture scheme of

Hsie et al, (1984) [6] has been substituted with a simplified version because the original scheme was computationally too expensive to be run in climate mode. In the simplified scheme only a prognostic equation for cloud water is included, which accounts for cloud water formation, advection and mixing by turbulence, re- evaporation in sub-saturated conditions, and conversion into rain via a bulk auto- conversion term. The main novelty of this scheme does not reside of course in the simplistic micro-physics, but in the fact that the prognoses cloud water variable is directly used in the cloud radiation calculations. In the previous versions of the model, cloud water variables for radiation calculations were diagnosed in terms of the local relative humidity. This new feature adds a very important and far reaching element of interaction between the simulated hydrologic cycle and energy budget calculations.

Changes in the model physics include a large-scale cloud and precipitation scheme which accounts for the subgrid-scale variability of clouds, new parameterizations for ocean surface fluxes, and a cumulus convection scheme. Also new in the model is a mosaic-type parameterization of subgrid-scale heterogeneity in topography and land use. Other improvements in RegCM3 involve the input data. The USGS Global Land Cover Characterization (GLCC) and Global 30 Arc-Second Elevation (GTOPO30) dataset are now used to create the terrain files. In addition, NCEP and ECMWF global reanalysis dataset are used for the initial and boundary conditions. The RegCM3 modeling system has four components: Terrain, ICBC, RegCM3, and Postprocessor. Vertical interpolation from pressure levels to the σ - coordinate system is performed in RegCM3 (see RegCM3 manual for more detail). The analysis domain can be set-up in any region of interest. The

model is possible to run for a day to long− term (up−to 2100) and outputs are available in 3-hour interval.

In general, RegCM3 is a complex system that contains many components such as inputs, numerical algorithms, and physical parameterizations, as well as chemistry. The performance of RegCM3 is inevitably subject to uncertainties caused by such components. In addition, uncertainties in RegCM3 are also caused by a number of external factors, e.g., choice of domain size and location, and choice of resolution. It is thus of interest here to investigate how the model physics, modeling options, and resolution influence the results of RegCM3 simulations.

3.2 Experimental setup

In this study the RegCM3 is nested with in ERA-INTERIM, ERA40 and NNRP1 reanalysis which provide initial conditions (ICs) and exponential lateral boundary conditions (LBCs). Sea surface temperature are used as surface boundary conditions. For the ICs and LBCs quantities each reanalysis dataset is interpolated to the grid of the RegCM3 and the first set of interpolation fields is used as ICs for the simulation. The physics of convective precipitation scheme used in this experiment is a Grell with the Fritsh and Chappell closure scheme.

The RegCM3 was run with the same horizontal resolution, 60km for a period of 10 years from 1989−1999 with the center of Addis Ababa, ETHIOPIA. The domain is 0 to 75 degree in the West-East direction and from -17 to 40 in the South-North direction.(i.e: 128 X 102 grid points, see Fig. 3.1).

The model is based on the primitive equations and a terrain following σ vertical coordinate system, where σ is given in Eq.(2.2.9) The vertical structure include 16 σ-levels above the surface. In its standard configuration RegCM3 use sea surface temperature(SST) from optical interpolation weekly (OI_WK).

An important requirement for RegCM3 is the availability of input data and the lateral boundary conditions (LBC) for the modeling period. The LBCs must be provided for the entire model integration period at 6-hour frequency.

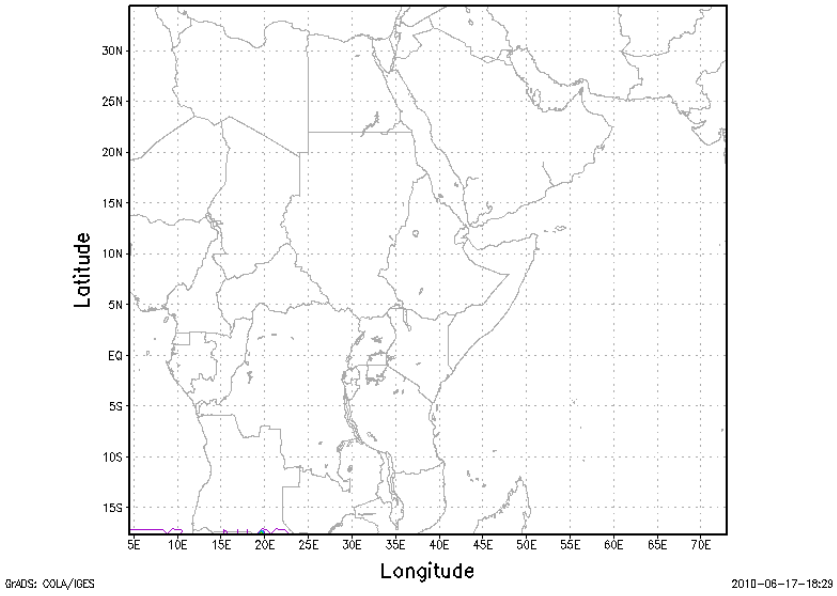

Figure 3.1: RegCM3 model domain. .

The RegCM3 run is performed three times by varying only the boundary forcing fields (ERA-40, ERA-INTERIM and NNRP1) keeping the other variables the same. The numerical value of the RegCM3 depends on the type of input data, domain size and time duration. Finally, the model output of mean monthly precipitation is compared with the observational precipitation over Ethiopia.

3.3 Boundary conditions

3.3.1 Surface boundary conditions

Orography is incorporated in the model as the lower boundary condition in a terrain following vertical coordinate system. Pressure has been widely used as a vertical coordinate in modeling and theoretical studies. Using pressure as an independent variable eliminates the not routinely observed air density from the governing equations in section 2 and simplifies thermodynamic equations. Furthermore, numerical models in such a coordinate system can easily incorporate observational data (CRU) that are generally available at pressure levels. There are however deficiencies of the sigma treatment of orography. This scheme may not handle sharp terrain gradients effectively. The orography data used in this study was taken from the global 2.5^0 horizontal resolution orography file archived at International Research Institute (IRI). This data was interpolated to the model horizontal grid resolution of 60 km using the linear interpolation scheme ([7] and reference therein). The land-use data adopted in the model was interpolated from 2.5^0 resolution data archived at National Centers for Atmospheric Research (NCAR). The time− dependent SST was interpolated from a $1^0 X 1^0$ grid of the monthly mean observed data. The surface pressure, air temperature, humidity are some of surface boundary condition variables.

3.3.2 Lateral boundary conditions

The RegCM3 has several options for lateral boundary conditions described in Anthes et al. (1987) [7]. However, in this study we have adopted the exponential relaxation method

([7] and reference therein). This scheme consists of Newtonian and diffusion terms that gradually drive the model solution of wind components, temperature, water vapor mixing ratio, and surface pressure toward specified large-scale values inside the lateral buffer zone. The lateral boundary condition variables are:

- Wind;
- Temperature;
- Water vapor; and
- Surface pressure.

As the size of the horizontal domain decreases, the specification of the velocity components and temperature along the boundaries affects the mean values of these quantities over the entire domain to an ever-increasing degree. Thus, on a mesoscale domain of 128 x 102, a set of boundary conditions may be computationally "stable" and produce "smooth" results, but even small errors in the treatment of precipitation, temperature or velocity may profoundly affect the mean kinetic and internal energy budgets over the domain.

These lateral boundary conditions were prescribed at every 1200 LST of integration using the European Center for Medium Range Weather Forecasting (ECMWF) reanalysis data (ERA40 and ERA−INTERIM) and National Center for Environmental Research and National Center for Atmospheric Prediction (NNRP1). In principle the replacement of the new GCM boundary conditions should be made at each time step, but studies by ([7] and reference therein) has shown that the error introduced by 12− hourly lateral boundary updates is negligible.

3.3.3 Initial conditions

Initial conditions in a numerical simulation represent the mean space-time characteristics of the atmosphere at the beginning of the numerical experiment. The model was initialized with the 12-hourly mean meteorological fields obtained from the ECMWF reanalysis and NCAR/NCEP reanalysis [7].

3.4 Area of study

Domain of simulation covers the whole Horn of Africa and the domain of the study is the whole Ethiopia which is located within latitudes of 3^0N to 18^0N and longitudes of 33^0E to 48^0E . Ethiopia is located in the Horn of Africa and bordered on the North and Northeast by Eritrea,on the East by Djibouti and Somalia, on the South by Kenya, and on the West and Southwest by Sudan. The country has a high central plateau that varies from 1,290 to 3,000 m (4,232 to 9,843 ft) above see level, with the highest mountain reaching 4,533 m (14,872 ft). Elevation is highest just before the point of descent to the Great Rift Valley. The country shares a total length of 5,260 km of international borders with its neighbors and has a total area of about $1,106,000 km^2$. It is bigger than all its neighbors except the Sudan and its east west distance (15^0) is longer than the northsouth distance (12^0).

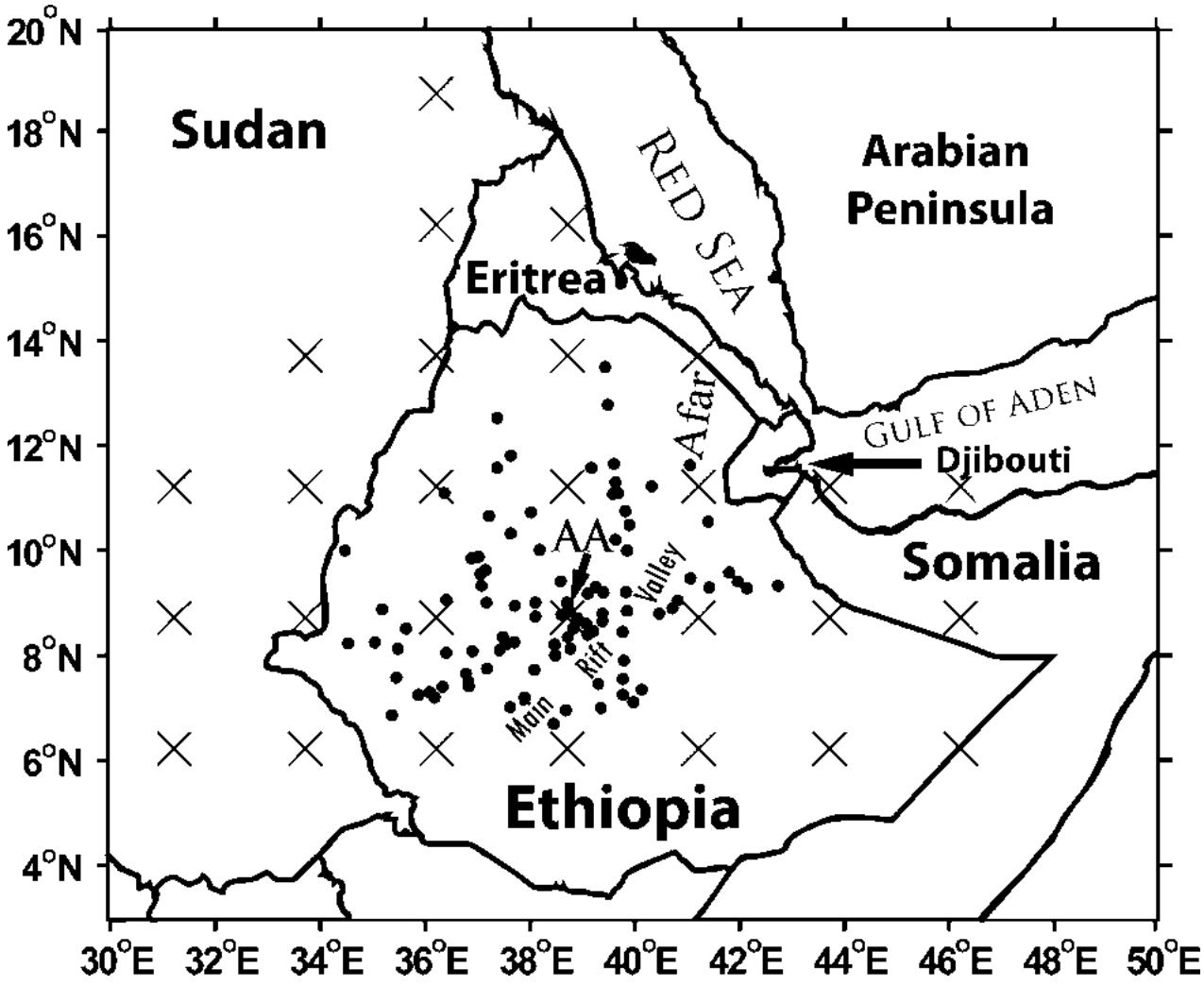

Figure 3.2: The geographic location of Ethiopia .

Chapter 4

Data and methodology

4.1 Global reanalysis datasets

4.1.1 NCEP/NCAR (NNRP1)

The NCEP/NCAR reanalysis data set is joint analysis between the National Center for Environmental Prediction (NCEP) and the National center for Atmospheric Research (NCAR). The main objective of this joint effort is to produce new atmospheric analysis using historical data from 1948 to present and as well to produce analysis of the current atmospheric state. This has two reanalysis dataset. These are NNRP1 and NNRP2. In this thesis only NNRP1 reanalysis dataset is used [8].

The NCEP /NCAR dataset consists of a reanalysis of the global observational network of meteorological variables (wind, temperature, geopotential height, humidity on pressure levels, and surface and flux variables) with the "frozen" state-of-the-art analysis and forecast system of the NCEP at a triangular spectral truncation of T62 [8]. Data are reported on a $2.5^0 X 2.5^0$ grid every 6 hours (00.00, 06.00,12.00 and 18.00 UTC), on 17 pressure levels from 1000hPa to 10 hPa. RegCM3 simulation used air temperature, surface pressure, relative humidity, soil moisture.

4.1.2 ERA-40

ERA-40 is a re-analysis dataset of Meteorological observation produced by the European Center for Medium-range Weather Forecasts (ECMWF) over the period from 1957 to 2002, when a major importance was made to the atmospheric observing system . ERA-40 produce analyses with six hourly frequency throughout the period, supplemented by intermediate three-hour forecasts. The products are of high temporal and spatial resolution, with a grid-spacing close to 125 km in the horizontal and with eleven levels in the vertical located between the surface and a height of about 65 km. The basic analyses variables will include the conventional meteorological wind, temperature and humidity fields, stratospheric ozone, ocean-wave and land uses. Additional information is produced concerning the quality of both the observations used and the analyses generated [9].

ERA-40 adopt innovative analysis techniques, especially with respect to satellite data, and use new types of observation and improved specifications of sea-surface temperatures and sea-ice distributions. It is built on experience gained earlier in carrying out re-analysis in Europe and the USA, and will deliver products that are unique in their combination of time-range, vertical extent, variety and accuracy. The RegCM3 simulation providing ERA40 use the atmospheric variables are evaporation, eastward surface stress, latent heat flux, ice surface temperature, 2 m temperature, etc [8].

4.1.3 ERA-INTERIM

After completion of ERA-40, effort was devoted to development of a new reanalysis system derived from the latest version of the operational ECMWF system. In 2006 a new reanalysis was started from January 1989, to produce an interim reanalysis (ERA-Interim) for the data−rich 1990s and 2000s, to be continued as an ECMWF Climate Data Assimilation System (ECDAS) until superseded by a new extended reanalysis. The main advances of the ERA-Interim data assimilation over the ERA-40 system are: 12 hour 4D-Var, T255 horizontal resolution, better formulation of background error constraint, new humidity analysis, improved model physics, quality control of data drawing on experience from ERA-40 and variational bias correction of satellite radiance data, improvements in radiosonde temperature and surface pressure bias handling, more extensive use of radiances, improved fast radiative transfer model and assimilation of rain affected Sea Surface Model (SSM) radiances through 1D-Var. ERA-Interim uses mostly the observations prepared for ERA-40 supplemented by data for later years from ECMWFs operational archive. Boundary forcing fields are taken from ERA-40 until 2002, and from ECMWF operations for later dates. However a few new dataset have been acquired [10].

The ERA-INTERIM is a reanalysis of the global atmosphere covering the data-rich period since 1989, and continuing in real time. As ERA-Interim continues forward in time, updates of the Archive will take place on a monthly basis.

The ERA-INTERIM project was initiated in 2006 to provide a bridge between ECMWFs previous reanalysis, ERA-40 (1957-2002), and the next-generation extended reanalysis envisaged at ECMWF [11]. The main objectives of the project were to improve on certain

key aspects of ERA-40, such as the representation of the hydrological cycle, the quality of the stratospheric circulation, and the handling of biases and changes in the observing system. These objectives have been largely achieved as a result of a combination of factors, including many model improvements, the use of 4-dimensional variational analysis, a revised humidity analysis, the use of variational bias correction for satellite data, and other improvements in data handling.

The atmospheric model is coupled to an ocean-wave model resolving 30 wave frequencies and 24 wave directions at the nodes of its reduced one-degree latitude/longitude grid. The main characteristics of the ERA-Interim system and many aspects of its performance are described in ECMWF. With some exceptions, ERA-Interim uses input observations prepared for ERA-40 prior to 2002, and for ECMWFs operational forecast system there after. The RegCM3 simulation use air temperature, surface pressure, relative humidity, eastward wind and soil moisture for this data.

4.2 Sea surface temperature data

Sea surface temperature (SST) is an important variable of the state of the Earth′s climate system. Thus, accurate knowledge of SST is essential for climate prediction. SSTs are also used as a surface boundary condition for numerical weather prediction and for other atmospheric model simulations. There are many different SST analyses produced throughout the world that resolve different temporal and spatial scales and use different sets of satellite and/or in situ data. In this paper we focus on climate-scale analyses, which we define as spatial scales of 1^0 grid and is 1 week time. Here we discuss about

the weekly optimum interpolation (OI) spatial scales at the National Oceanic and Atmospheric Administration.

The optimum interpolation (OI) sea surface temperature (SST) analysis is produced weekly on a one-degree grid. The analysis uses in situ and satellite SST's plus SST's simulated by sea-ice cover. The dataset used in the netCDF files format are the data of the beginning of the 7-day average period. For the more recent period, 1990-present, the weeks are defined to be centered on Wednesday. During the period 1981-1989, the weeks are centered on Sunday. The latitude/longitude values in the netCDF coordinate variables are the centers of the grid cells.

The OI analysis is done over all ocean areas and the Great Lakes. There is no analysis over land. The land values are filled by a Cressman interpolation to produce a complete grid for possible interpolation to other grids. The ocean and land areas are defined by a land sea mask. Land values for SST do not necessarily coincide with land values from ice analysis [12].

4.3 Observation data

In this study we used observational dataset from climate research unit (CRU). It is a station data over the land for precipitation and temperature in the period from 1960 to 2000. CRU has developed a number of data sets widely used in the climate research including the global temperature and precipitation used to monitor the state of the climate system as well as numerical and dynamical climate model simulation.

The CRU global climate dataset, available through Intergovernmental Panel on Climate Change (IPCC) Data Device Channel (DDC) consists of 1^0 latitude by 1^0 longitude resolution mean monthly climatology for global land use. The mean climatology comprises eleven surface variables, such as precipitation, maximum and minimum temperature, vapor pressure, cloud cover, etc [13].

4.4 Analysis of RMSE, bias and correlations

The performance of RegCM3 over different part of Horn of African region for rainfall pattern during $1989-1998$ simulation period is determined by analysis of the bias, the root mean square error (RMSE) and correlation of the simulated and observed precipitation [2]. The bias is a time average of the error defined as:

$$bias = \frac{\sum_{i=1}^{N}(ppt^M - ppt^O)}{N} \tag{4.4.1}$$

Root mean square error (RMSE) is a measure of the square difference between the RegCM3 simulated precipitation and observed precipitation values at each cluster (grid point). If ppt^M and ppt^O are the RegCM3 and observed field the RMSE can be estimated using the relationship

$$RMSE = [\frac{\sum_{i=1}^{N}(ppt^M - ppt^O)^2}{N}]^{1/2} \tag{4.4.2}$$

where the simulation is carried out over N grid points in a predefined region and the superscripts M and O refers to model and observation. The model performance is evaluated by comparing the mean simulated rainfall with the corresponding observational rainfall pattern. Systematic RMSE represents the error that is similar at all points in the gridded data. Accurate models have low systematic RMSE [7].

Simple correlation analysis can be used to determine the degree of linear relationship between the RegCM3 precipitation providing the three boundary forcing field and the observational precipitation over Ethiopia. For any month k, simple correlation coefficient r_k between the RegCM3 precipitation, M and observational precipitation, O can be expressed as

$$r_k = \frac{\sum_{k=1}^{N}(M_k - M')(O_k - O')}{[(\sum_{k=1}^{N}(M_k - M')^2)(\sum_{k=1}^{N}(O_k - O')^2)]^{1/2}} \tag{4.4.3}$$

where N is the total number of records, M' and O' are a long tern mean of RegCM3 and observation, respectively. The value of r_k is between -1 and 1. positive and negative values of r_k are indicative of the positive or negative relationships, respectively [7].

4.5 Rotated principal component analysis (RPCA)

Rotated Principal Component Analysis (RPCA) analysis is the most efficient way of compressing geophysical data both in space and time, as well as separating noise from meaningful data. It enables fields of highly correlated data to be represented adequately by a small number of orthogonal functions and the corresponding orthogonal time coefficients, which account for much of the variance in their spatial and temporal variability. EOF techniques are used to extract from a covariance matrix, robust structures that explain the largest variance of the original matrix and at the same time are uncorrelated. The original data is split into orthogonal spatial patterns (eigenvectors) and corresponding time series coefficients (principal components). An eigenvector pattern that accounts for a large function of the variance (eigenvalues) is considered to be physically meaningful. Kutzbach (1967), and Storch and Zwiers (1999) [7] have provided a lucid outline of the

mathematical procedure necessary to define the functions and their time coefficients. In this study, the EOF method was applied on seasonal rainfall anomaly using the mathematical formulation described in Peixoto and Oort (1992) [7]. The following steps are followed in this procedure:

(a) Define a geophysical fluid matrix, F_{MXN} whose elements (f_{mn}) are standardized values, where m=1,2,...M, (observational points) and n=1,2,....N, (time i.e. months, years, seasons etc.).

(b) Compute the covariance matrix R_{MXM},

$$R = \frac{1}{N} F F^T \tag{4.5.1}$$

(c) Determine the eigenvectors E=[e1,e2,.....eM] and the eigenvalues l=[l1,l2,.....lM] from the characteristic equation of R, where

$$(R - \lambda I) = 0 \tag{4.5.2}$$

and I is a unit matrix.

(d) Compute the principal component time series, C such that its elements C_{MN} are the projection of $f_{_N}$ on e_M given by

$$C = E^T F \tag{4.5.3}$$

Rotation of EOF has the effect of redistributing the variance within the eigenvectors and therefore removing the ambiguities while conserving the variance extracted by the selected subset of non−rotated eigenvectors. Various methods of determining the number of significant EOF modes to retain for rotation have been discussed ([7] and reference

therein) have suggested the use of sampling errors in determining the number of significant eigenvectors. The sampling error test is based on comparison of sampling errors for the eigenvalues and the amount of separation from the neighboring eigenvectors. If the sampling errors in the eigenvalues are comparable to the distance from the nearby eigenvalue, then the sampling errors in the EOF will be comparable to the nearby EOF. In this study the criteria of North et al. (1982) and Kraiser (1959) [7] were used in determining the number of dominant EOF modes to be retained and rotated.

Annual and seasonal rainfall patterns over Ethiopia are very complex due to the existence of complex topography and large inland water bodies. EOF analysis were used to delineate homogeneous climate regions in Ethiopia using mean monthly rainfall data of CRU. The method used in this analysis is a modified version of the technique employed by Ogallo (1988) and similar to the one adopted by Dyer (1977) [7]. Delineation of a homogeneous area was accomplished by identifying the cluster with the largest correlation with the Principle Component (PC) time series associated with the first eigenvector of the annual rainfall anomaly. For this particular study only four clusters were found to cover the whole country (see Fig. 5.2).

Chapter 5

Result and discussion

This chapter deals with elaborations of the results that are obtained from the RegCM3 simulation using the three different boundary forcing dataset. The results are compared with CRU precipitation for Ethiopia as a whole and to mean CRU precipitation over 4 homogeneous regions of the country. The four climatological homogeneous regions are identified from analysis of CRU precipitation based on Rotated Principal Component Analysis (RPCA) as indicated in chapter 4.

5.1 Mean climatology

The main performance of RegCM3 over our domain for the three boundary forcing fields can be seen in Fig. 5.1. The first column refers to RegCM3 simulation of precipitation with the rows under this column representing simulated precipitation under boundary forcing field of ERA40, ERA−INTERIM and NNRP1 respectively. The second column represents CRU precipitation while the third column represents difference between RegCM3 and CRU precipitation covering only latitude − longitude of Ethiopia for clarity averaged over the period covering 1991.

Comparison of rows of the third column reveals that simulation based on ERA−INTERIM

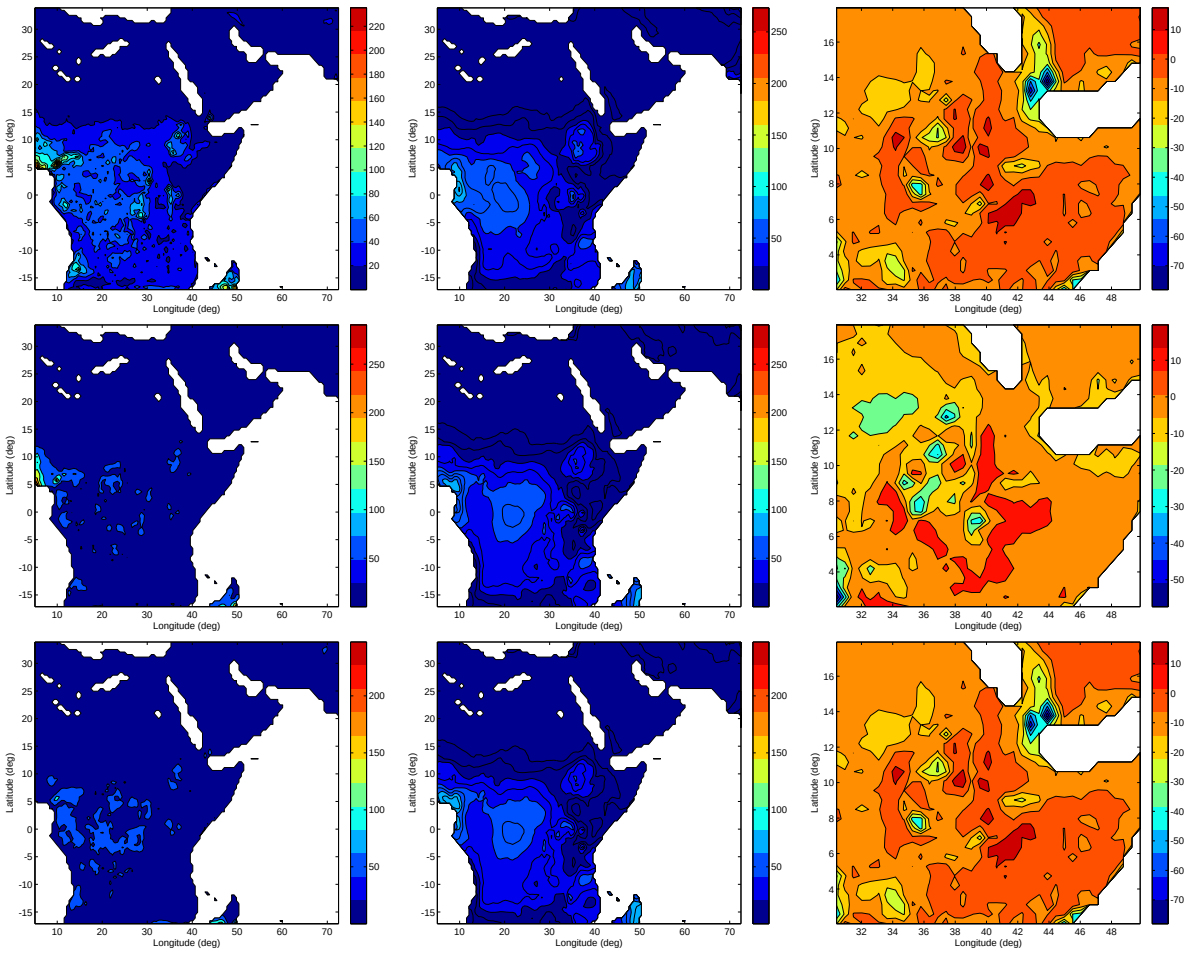

Figure 5.1: Comparison between RegCM3 simulated rainfall using different global re−analysis dataset as boundary forcing and CRU precipitation averaged over the period covering 1991 over the domain of simulation .

exhibit better agreement with CRU precipitation particularly over Ethiopia. However, simulation of precipitation based on all three forcing fields show higher precipitation than CRU precipitation over the highlands of Ethiopia and lower precipitation than CRU over lowland areas. More detailed analysis of the impact of the boundary forcing fields on RegCM3 simulation over smaller Ethiopian domain (0^0-20^0N and 30^0-50^0E is performed. On the basis of RPCA, this domain is clustered into 10 regions by the 1^{st} 10 EOFs explaining over 83% variance in CRU precipitation, however, only 4 of these lies within Ethiopia. These are cluster 1 (left top), cluster 2 (right top), cluster 4 (bottom left), and cluster 5 (bottom right) as shown in Fig. 5.2. The Empirical Orthogonal Function (EOF) describing this region accounts for 23%, 21%, 6%, 5% of the total CRU precipitation variability.

The first EOF describes the lowland of South−Eastern, the second EOF covers Western, South−Western and North−Western, the third EOF covers central and South−Eastern highland and the forth EOF describes the Southern part of Ethiopia.

Figs. 5.3−5.5 show that the scatter plot of CRU versus simulated rainfall for the selected 4 clusters based on ERA40, ERAIN and NNRP1 respectively. The four panels in Fig. 5.3 shows compact linear relation for cluster top−right panel while the rest are some what scattered.

The RMSE is 0.5−1.5 mm/day for all 4 clusters. The bias is mostly positive except for a negatively biased cluster 2 (see Fig 5.6 left panel). Fig. 5.4 shows better relationship between CRU rainfall and RegCM3 rainfall exhibiting fairly linear relationship for all of the clusters. The worst relationship between CRU observation and RegCM3 simulation can

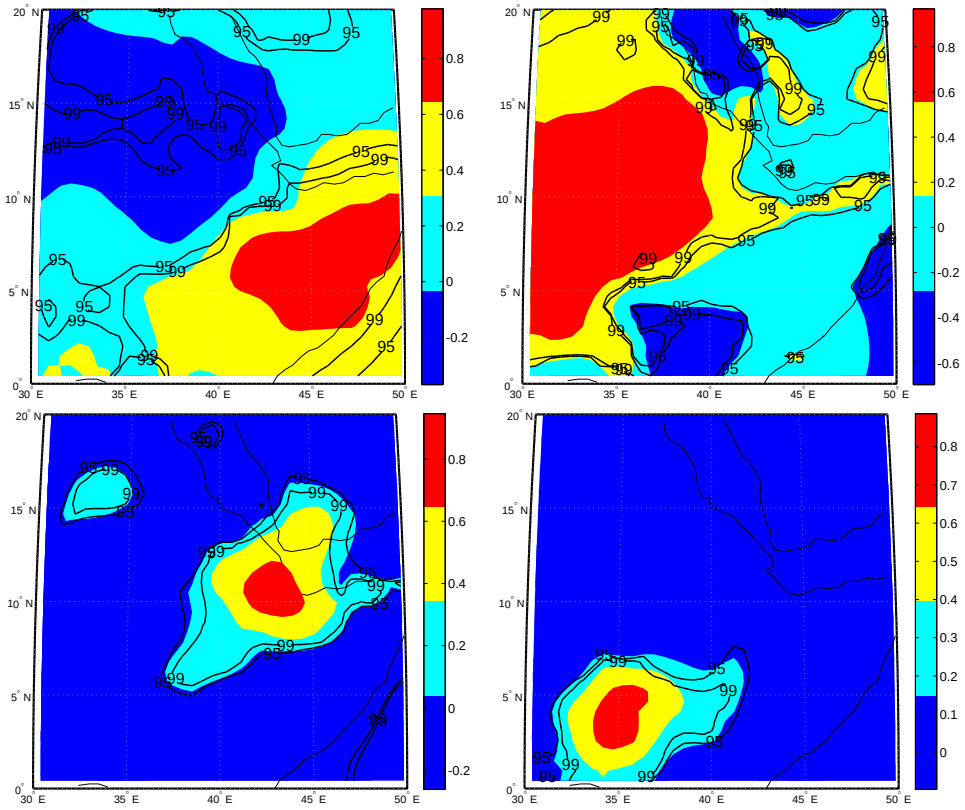

Figure 5.2: Clustering of homogeneous model grids over Ethiopia. Top−left: cluster 1;Top−right: cluster 2; Bottom−left: cluster 4; and Bottom−right: cluster 5.

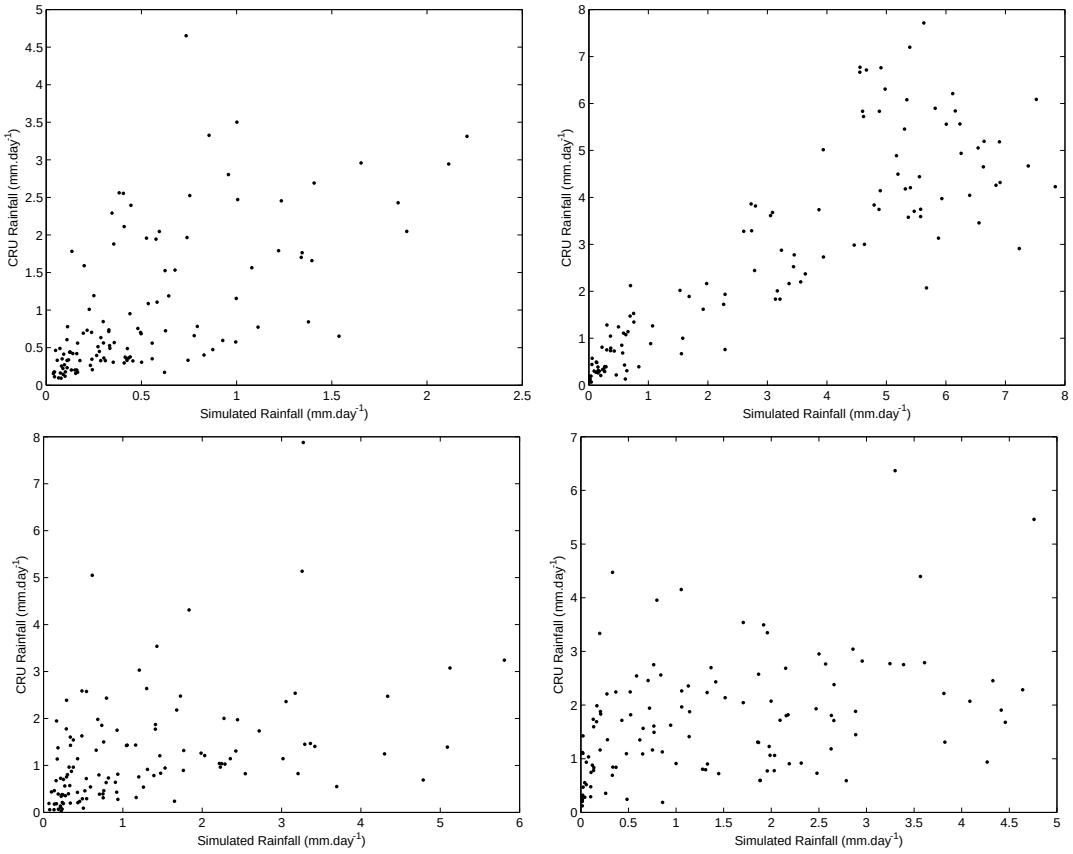

Figure 5.3: The relationship between CRU and RegCM3 rainfalls, distribution based on ERA−40 over Ethiopia in the 4 clustered regions. Top−left: cluster 1;Top−right: cluster 2; Bottom−left: cluster 4; and Bottom−right: cluster 5

be seen in bottom−right panel of Fig. 5.3. RMSE for simulation using ERA−INTERIM is of the same order in general eventhough there is a slight improvement from ERA40. The precipitation bias is positive for all the homogeneous region (clusters) in contrast to some negative bias for ERA40 (see Fig.5.6, right panel). Fig 5.5 shows comparison between rainfall simulated by RegCM3 and CRU rainfall for NNRP1 dataset. The relationship shown in the 4 upper panels are as good as what we found for ERA−INTERIM. quantitatively, we found that RMSE is slightly higher than that of ERA−INTERIM. The bias analysis also reveals that NNRP1 dataset generally forces RegCM3 towards negative bias compared to CRU rainfall (see Fig. 5.6, Bottom panel).

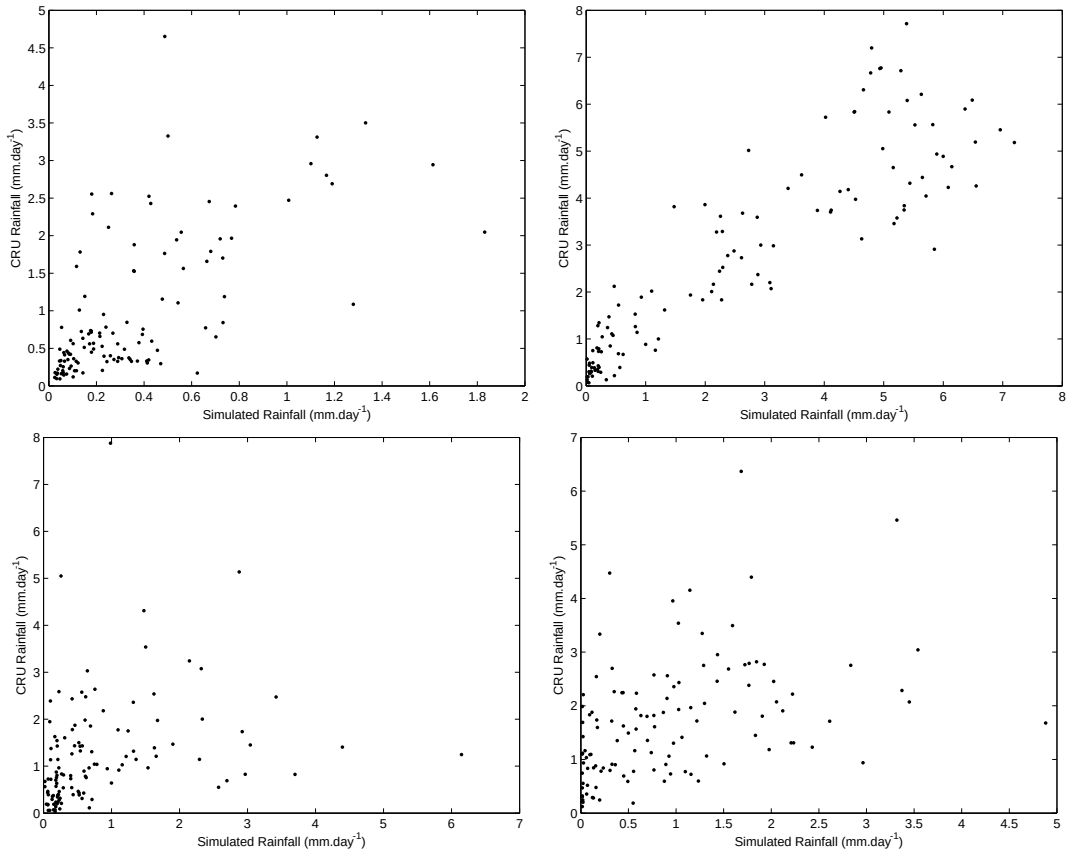

Figure 5.4: The relationship between CRU and RegCM3 rainfalls, distribution based on ERA−INTERIM over Ethiopia in the 4 clustered regions. Top−left: cluster 1;Top−right: cluster 2; Bottom−left: cluster 4; and Bottom−right: cluster 5.

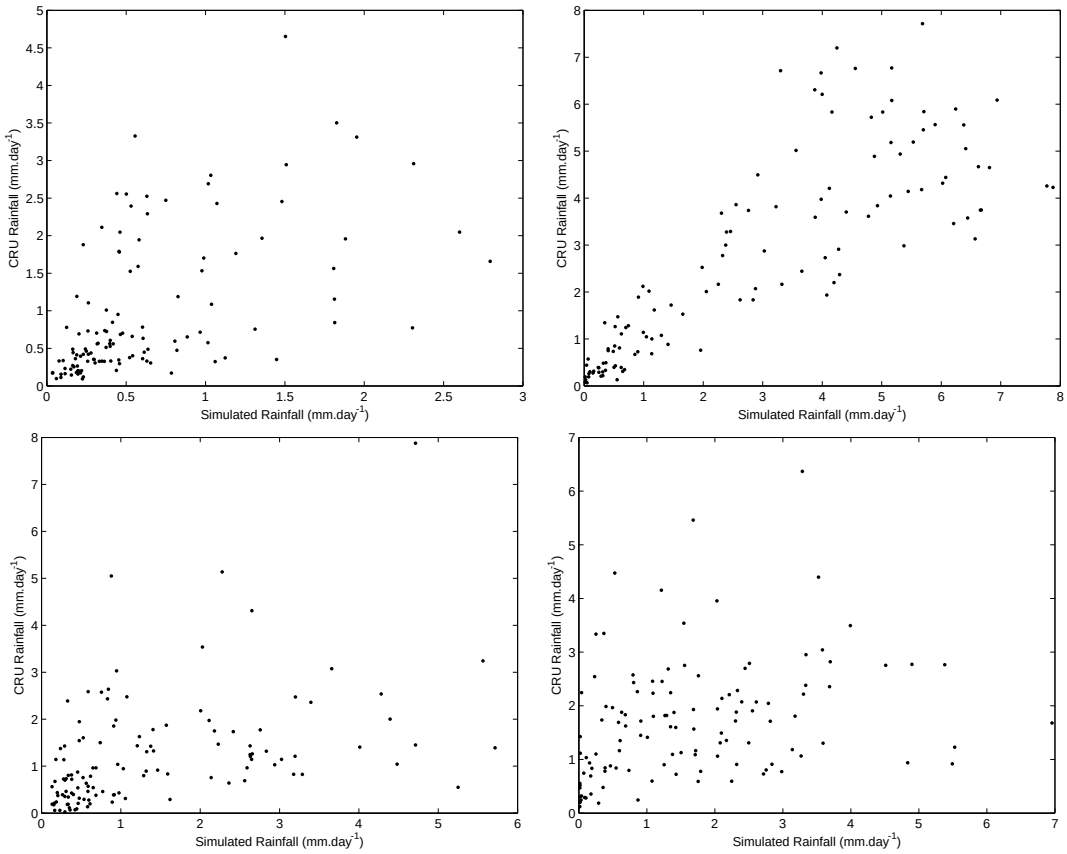

Figure 5.5: The relationship between CRU and RegCM3 rainfalls, distribution based on NNRP1 over Ethiopia in the 4 clustered regions. Top−left: cluster 1;Top−right: cluster 2; Bottom−left: cluster 4; and Bottom−right: cluster 5.

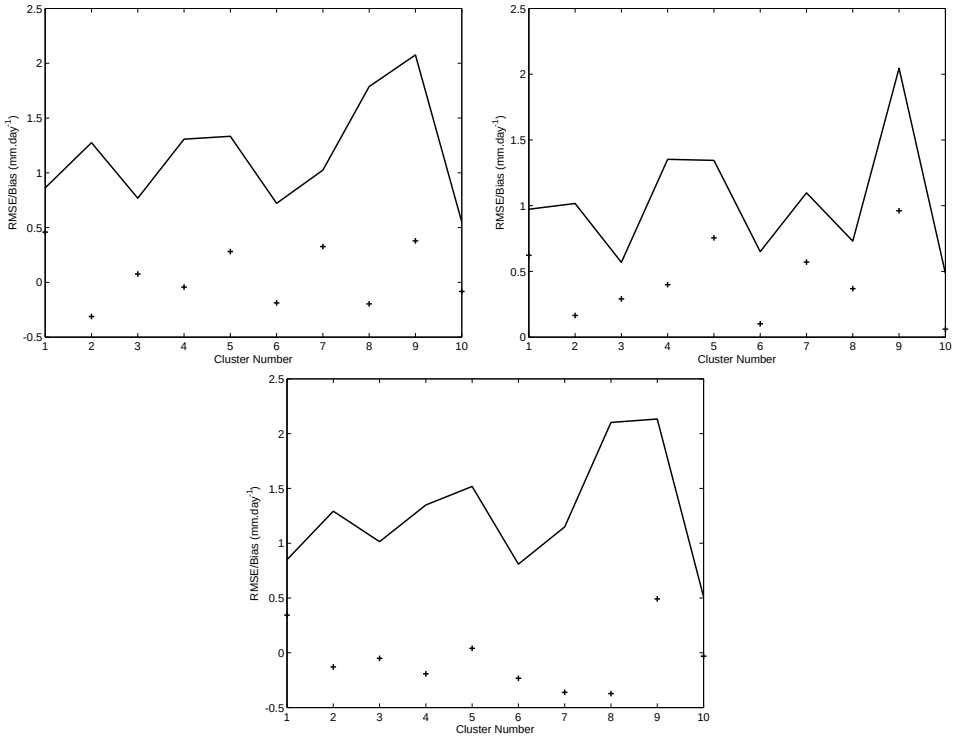

Figure 5.6: The relationship RMSE and bias versus each clusters. Top−left panel: ERA40; Top−right panel: ERA−INTERIM and Bottom panel: NNRP1.

5.2 Large scale features

Because intra-seasonal and inter-annual variability in regional atmospheric circulations modulate local rainfall, an overview of the regional circulation climatology as captured by RegCM3 is given to provide the larger-scale context that produces rainfall over the Horn of Africa. The most important circulation features and patterns are briefly described below.

5.2.1 Inter tropical convergence zone (ITCZ)

The Inter Tropical Convergence Zone (ITCZ) is the region where the Northeasterly and Southeasterly trade winds coverage, forming an often continuous band of clouds near the equator. Usually it is located between $2^0 - 3^0$ latitude just between two Hadley cell and

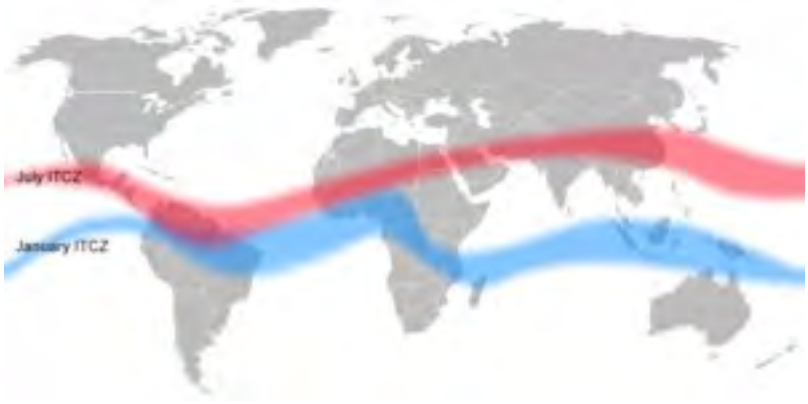

Figure 5.7: Position of the ITCZ in July (red) and in January (blue) over the tropical regions (Source: www.weather.gov) .

serves as a convergence between the two. It is a lower layer of the atmosphere which separates the dry Northeast trade wind from the moist South Easterlies. The cloud formation and the seasonal rainfall pattern are affected by the migration of the ITCZ in the North−South direction over east Africa. Cloud formation and weather activities are located 200−500km behind the surface of ITCZ.

The position of ITCZ is varied based on the change of high and low pressure cell and the apparent movement of the sun. The position of ITCZ is quasi−permanent and the interannual oscillation of the surface position of the ITCZ causes a variation in the wind circulation patterns over Ethiopia ([15] and reference therein). By using RegCM3 boundary forcing fields of annual mean wind reanalysis data over the period 1989 − 1999, we see the position of ITCZ changes during seasons over the simulated region. Its migration alternatively causes the onset and withdrawal of seasonal winds from North and South. During the summer season the sun is overhead North of equator, but during dry season ITCZ is just North of Ethiopia. An Indian and Atlantic oceans are the main source of rainfall. The main source being the Atlantic, the winds responsible for the rain

are the Guinea monsoon and the South easterlies. The rain covers most parts of Ethiopia except the South Eastern Lowlands and the Afar Depression. The length of the rainy season varies from place to place depending on the length of the predominant wind. On the contrary, during the Bega season, the ITCZ is North of the equator. The high pressure cell develops over the dry air masses originating either from the Saharan anticyclone (high pressure) or the south west Asia and the low pressure cell (cyclone) in central Africa. The ITCZ lies far south of Ethiopia and the North Easterlies cool dry winds, whose origin is the Asian land mass, predominate over most parts of Ethiopia. As these winds bring no or little moisture, most parts of Ethiopia remain dry.

5.2.2 Subtropical jet stream (STJ)

Subtropical jets, are best developed in winter and early spring. During summer, in the Northern Hemisphere, the subtropical jet weakens considerably, During winter, subtropical jets intensify and can be found between 20^0 and 50^0 latitude. The core is most frequently found between 35,000 and 40,000 feet. A subsidence motion accompanies subtropical jets and gives rise to predominantly fair weather in areas they pass over. These jets are also remarkably persistent from time to time, but they do fluctuate daily. Sometimes they drift Northward and merge with a polar−front jet. Over Asia in summer, the subtropical jet is replaced by the tropical Easterly jet stream. The seasonal variation in the strength is captured by all three simulations. The STJ strength reaches maximum in February for all three simulations of boundary fields over Ethiopia ([16] and reference therein).

5.2.3 Tropical easterly jet (TEJ)

Tropical Easterly jet occur near the troposphere over Southeast Asia, India, and Africa during summer. The strongest winds are over Southern India, but they are not as intense as the winds encountered in polar-front or subtropical jet streams. This jet is closely connected to the Indian and African summer monsoons. The existence of this jet implies that there is a deep layer of warm air to the North of the jet and colder air to the South over the Indian Ocean. This warm air is of course associated with the maximum heating taking place over India in summer, while the colder air is over the ocean. The difference in heating and cooling and the ensuing pressure gradient is what drives this jet .

During Ethiopian Kiremt, this jet carries moisture from the Indian Ocean and enhances the rainfall in the country ([17] and reference therein). All the RegCM3 simulations captured TEJ, though there is difference in the strength and position of TEJ from one simulation to the other. The seasonal variation in the strength of TEJ is also captured by all three simulations. The TEJ strength reaches its peak in July as depicted in Fig. 5.7 for all simulations on the three dataset for boundary forcing.

As TEJ is a strong wind it can facilitate the development of summer storm when low level conditions are fulfilled. Its development and persistency play a great role in enhancing rains over major rain getting regions of Ethiopia during the kiremt months. Therefore assessing the performance of RegCM3, upon use of different forcing fields with respect to capturing large scale meteorological features is a crucial scientific topic.

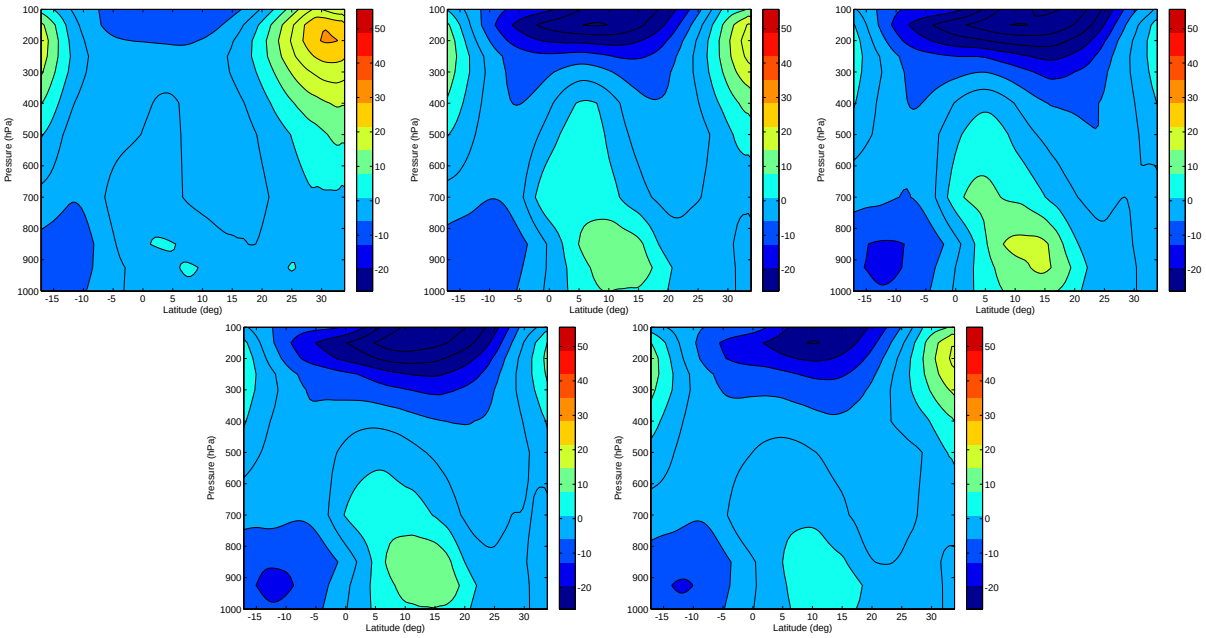

Figure 5.8: Formation of Atmospheric circulation such as STJ, TEJ and lowlevel SJ over Ethiopia of month May, June, July, August and September for ERA40 simulation from top left to right, respectively. Color representation: black STJ, Orange TEJ and Grey SJ .

5.2.4 Somali jet (SJ)

Somali Jet (SJ) is a low-level southwesterly jet over the Arabian Sea in the summer months, off the coast of Somalia. It is the northern branch of a cross-equatorial flow, giving rise to a major supply of moisture in support of the Asian summer monsoon. The north/south branch of the jet begins to form as early as April when the East African equatorial winds shift abruptly from easterly to southerly, transporting mass and moisture across the equator and into Southern Ethiopia.

The time of onset of the Somali jet when wind speed is $12ms^{-1}$ in the western Arabian sea ([18] and reference therein). The SJ can be seen in all simulations as shown in Fig 5.8 for ERA40. The SJ strength reaches its peaks in July for all simulations.

5.3 Inter−annual variation

Ethiopian climate varies according to the different topographical regions. The central plateau has a moderate climate with minimal seasonal temperature variation. The mean minimum temperature during the coldest season is 4^0C , while the mean maximum rarely exceeds 27^0C. Temperature variations in the lowlands are much greater, and the heat in the desert and Red Sea coastal areas is extreme, with occasional highs of 60^0C. Heavy rainfall occurs over most of the country during June, July, and August and High Plateau also experiences a second, though much milder, rainy season between December and February throughout the year.

Fig 5.9 show the correlation between CRU rainfall and RegCM3 simulations based on different forcing fields (first row: ERA40, second row: ERAIN and third row: NNRP1) for the months of Jun, July and August from left to right for the whole simulated period , respectively. The significance of the correlation is nearly 100% as shown by plus mark in the same figure for three boundary fields. There is interannual variation in the performance of RegCM3 simulations for all boundary forcing fields. The interannual variations in the correlation of RegCM3 precipitation with CRU is maximum in the month of June for all boundary forcing fields. However, simulation of rainfall based on ERA−INTERIM dataset exhibits better agreement with CRU through the simulation years and for all the month. ERA40 dataset seems to perform better than NNRP1 with respect to consistency of correlation with observations from year to year [14].

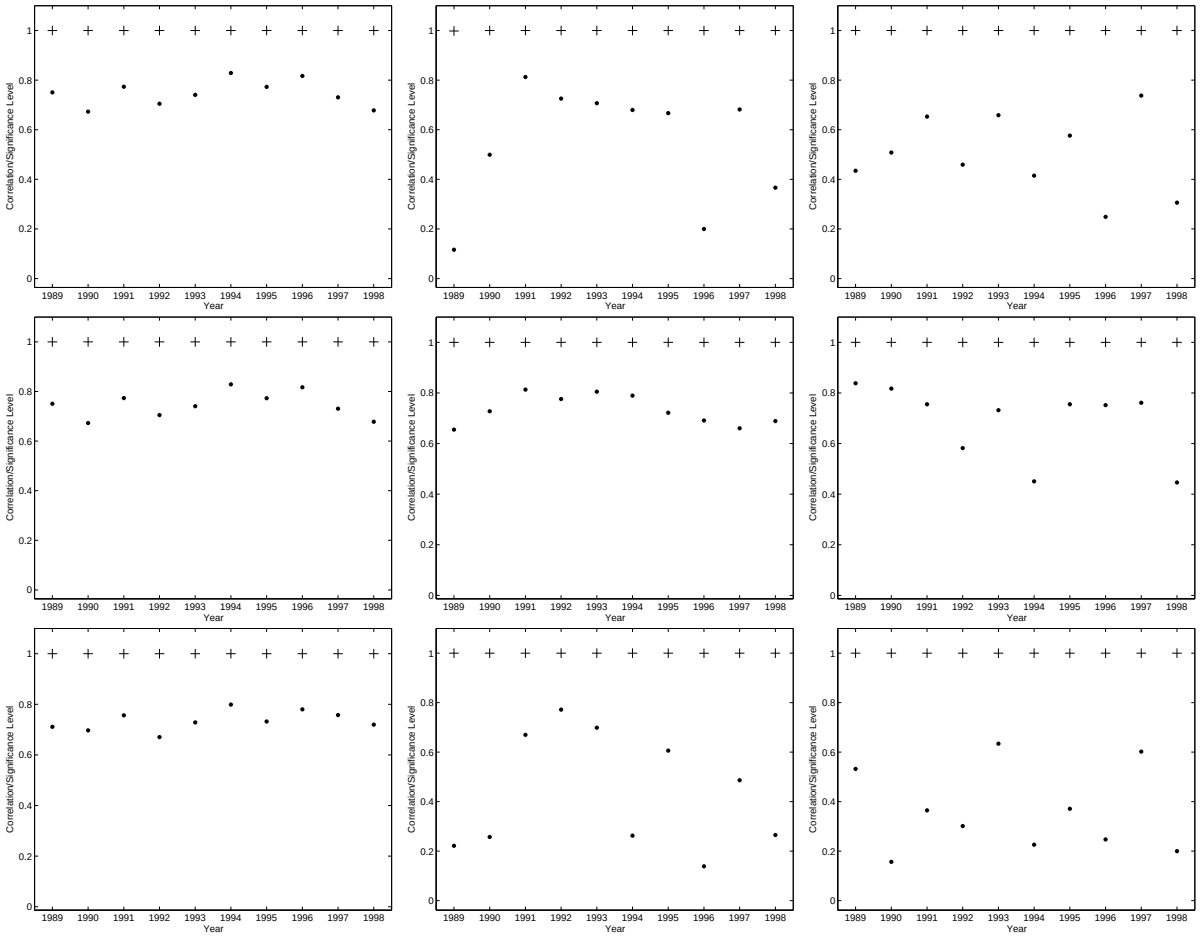

Figure 5.9: Correlation of RegCM3 and CRU rainfalls for the simulation period 1989−1999 over Ethiopia for Kiremt (JJA months from left to right, respectively) and for ERA40, ERA−INTERIM and NNRP1 from top to bottom respectively.

5.4 Intraseasonal variation

Correlation and significance level analyses are used to identify the best boundary forcing fields over Ethiopia. Barnston et al (1996) demonstrated that the time−space behavior of the SST field alone influences the seasonal rainfall in certain region/seasons for Africa, both on inter−annual and intra−seasonal variability. For Ethiopia, Segele and Lamb (2009) [19] examined the possible associations with ENSO and global SST for the onset and growing length of the main rainy season (kiremt). They found moderate to strong correlation between the commencement and duration of the season with Indian ocean and equatorial pacific ocean SSTs(+ 0.45 to 0.55,significant at the 100%). In similar, Gissila et al (2004) and Korecha and Barnston(2007) [19] used global SSTs to predict JJAS Ethiopian rainfall, and found significant associations with Indian and Pacific ocean. In this section we discuss the relationship between Ethiopian rainfall as obtained from RegCM3 simulation based on three global reanlysis dataset and CRU rainfall.

Fig 5.10 show the correlation between CRU and RegCM3 simulations based on different forcing fields (first row: ERA40, second row: ERAIN and third row NNRP1) for the months of November, December and February (NDF) respectively. The significance of the correlation is nearly 100% for ERA40, but ERAIN and NNRP1 for December below 100% as shown by plus mark in the same figure. There is inter−seasonal variation in the performance of RegCM3 simulations for all boundary forcing fields. This can be confirmed from comparing Fig 5.9 for JJA and Fig 5.10 for NDF. RegCM3 simulation performed much better for the Kiremt season than the Bega season. The intra−seasonal variability can be determined by investigating the variation from June to August for kiremt and

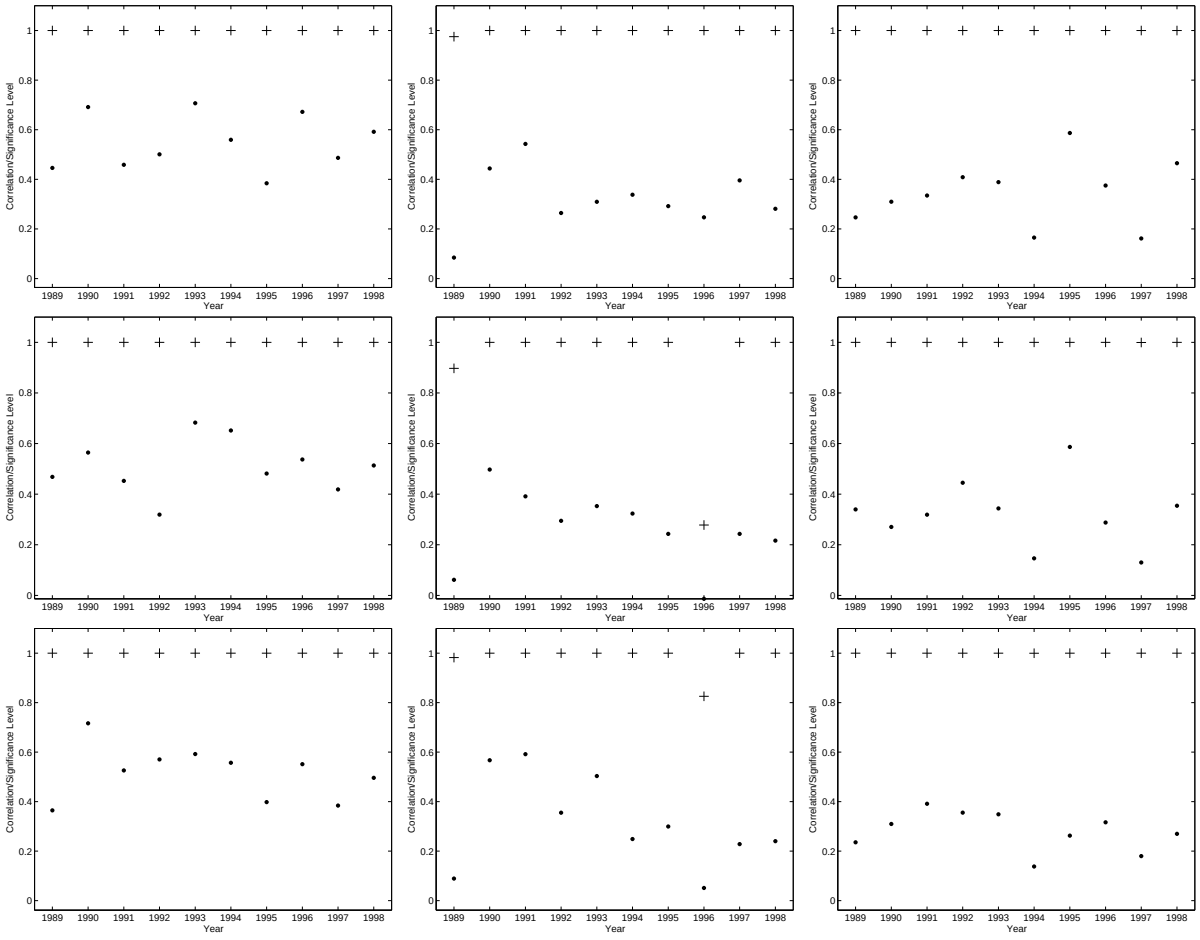

Figure 5.10: Correlation of RegCM3 and CRU rainfalls for the simulation period 1989−1999 over Ethiopia for Bega (NDF months from left to right, respectively) and for ERA40, ERA−INTERIM and NNRP1 from top to bottom respectively.

November to February for Bega as shown in Figs. 5.9−5.10 respectively. We have already seen the variation with in Kiremt that RegCM3 performs very well in June and gradually this performance decreases in August for all forcing fields. It is to be noted that ERA−INTERIM is better than the two other dataset in all the months.

Chapter 6

Conclusion

The performance of RegCM3 in capturing large scale climate features using the three boundary forcing dataset has been evaluated. It is found that RegCM3 simulation captures major large scale features such as Tropical Easterly jet (TEJ), Subtropical jet (STJ), ITCZ and Somali jet (SJ) under all boundary forcing fields. However, the performance of RegCM3, has improved a lot when ERA−INTERIM is used.

The performance of RegCM3 in capturing interannual, interseasonal and intraseasonal variability have been analyzed as indicated in chapter 5. RegCM3 rainfall simulations agrees well with CRU rainfall during the rainy season (JJA) and the agreement deteriorates during mostly dry period over Ethiopia (e.g. NDF) under all boundary forcing fields. However, use of ERA−INTERIM dataset for boundary forcing leads to improvement in reproducing observed rainfall throughout the year. The variation from month to month is similar to other fields with strong correlation between simulated and observed rainfall in June of every year.

The analysis is also made for average rainfall over the four selected homogeneous regions of Ethiopia. The agreement between observed and simulated rainfall under all boundary forcing dataset is found to be different from cluster to cluster. The 2^{nd} cluster

representing Western, South−Western and North−Western region of Ethiopia exhibited very good linear relationship between observed and simulated rainfall. This followed by the 1^{st} cluster, 5^{th} and 4^{rd} cluster in this order. The features are also reflected in calculated RMSE and bias for all boundary forcing fields. However, there is also difference among simulations from different forcing fields. It is noted that simulation using ERA−INTERIM is superior to the other two interms of both rainfall RMSE and bias. Both simulations from ERA40 and NNRP1 tend to show negative rainfall bias compared to CRU rainfall (some cluster for ERA40 and nearly all 10 clusters for NNRP1 dataset). Simulation based on ERA−INTERIM is characterized by positive rainfall bias and relatively smaller RMSE for some clusters particularly for those over Ethiopia.

In summer, our study has found that performance of RegCM3, constrained by ERAIN dataset, is far better than the other two boundary forcing dataset in simulating observation. In particular, the performance of RegCM3 in reproducing large scale features, mean climatology, variability at different time scales and rainfall is found to improve when the simulation is constrained by ERA−INTERIM dataset.

Bibliography

[1]. Mary-Jane Morongwa Kgatuke, August 2006: The internal variability of the regional climate model RegCM3 over southern Africa. *Ms.thesis*.

[2]. Zewdu T. Segele. 2009: Large-scale atmospheric circulation and global sea surface temperature associations with Horn of Africa June−September rainfall. *Int.J.* Climatol. 29: The University of Oklahoma, Norman, OK 73072, USA

[3]. Abera D., July 2007. Simulation of the effect of random geopotential height disturbance on air flow on a barotropic atmosphere using corase resolution grid. Ms thesis, AAU physics dept.

[4]. JAMES R. HOLTON., 2004: An introduction to drnamic meteorology. Fourth Edition, volum 88.

[5]. MARK Z. JACOBSON, 2005: Fundamentals of Atmospheric modeling. Second Edition, *textbook*. 1−168.

[6]. Nellie Elguindi, Xunqiang Bi, Filippo Giorgi, Badrinath Nagarajan, Jeremy Pal, Fabien Solmon, Sara Rauscher, and Ashraf Zakey, July 2000: RegCM Version 3.1 Users Guide. Trieste, Italy.

[7]. INDEJE, MATAYO., 2000: Prediction and Numerical Simulation of the Regional

Climate of Equatorial Eastern Africa. Marine, Earth and atmospheric science., USA

[8]. http://www.cpc.ncep.noaa.gov/preoducts/wesley/reanslysis.html.

[9]. http://www.ecmwf.int/research/era/era40survey/.

10]. http://www.ecmwf.int/research/era/do/get/era-interim.

[11]. P. A. Mooney, 2010: Comparison of ERA-40, ERA-Interim and NCEP/NCAR reanalysis data with observed surface air temperatures over Ireland. Int. J. Climatol. Department of Experimental Physics, NUI Maynooth, Kildare, Ireland. 1−13

[12]. http://www.cru.uea.ac.uk/cru/about/.

[13]. http://www.esrl.noaa.gov/psd/data/gridded/data.noaa.oisst.v2.html.

[14]. Sakari Uppala1, Dick Dee1, Shinya Kobayashi1,2 and Adrian Simmons1, 2006: Evolution of reanalysis at ECMWF. Japan Meteorological Agency, Japan.

[15]. Jones PD, Moberg A. 2003: Hemispheric and large-scale surface air temperature variations: An extensive revision and update to 2001. Journal of Climate 16: 206223.

[16]. Krishnamurti, T. N., 1961: The subtropical jet-stream of winter. J. Meteor. 18, 172-191.

[17]. Koteswarran, P., 1958: The easterly jetstreams in the tropics. Tellus. 10, 43-57.

[18]. Krishnamurti, T. N., Molinari, J., and H. L. Pan, 1976: Numerical simulation of the Somali jet. J. Atmos. Sci. 33, 2350-2362.

[19]. Zewdu T. Segele,nt. J. Climatol. 29, 2009: Evaluation and adaptation of a regional climate model for the Horn of Africa: rainfall climatology and interannual variability 1075−1100 .

Declaration

This thesis is my original work, has not been presented for a degree in any other University and that all the sources of material used for the thesis have been dully acknowledged.

Name: GIRMA MOLORO

Signature:

Place and time of submission: Addis Ababa University, July - 06 2010

This thesis has been submitted for examination with my approval as University advisor.

Name: Dr.GIZAW MENGISTU

Signature: